



Evaluation of the Glaucomatous Macular Damage by Chromatic Pupillometry

Yadan Quan · Huiyu Duan · Zongyi Zhan · Yuening Shen ·
Rui Lin · Tingting Liu · Ting Zhang · Jihong Wu · Jing Huang ·
Guangtao Zhai · Xuefei Song · Yixiong Zhou · Xinghuai Sun

Received: April 17, 2023 / Accepted: May 16, 2023 / Published online: June 7, 2023
© The Author(s) 2023

ABSTRACT

Introduction: This study aimed to examine the performance of binocular chromatic pupillometry for the objective and rapid detection of primary open-angle glaucoma (POAG), and to explore the association between pupillary light response (PLR) features and structural glaucomatous macular damage.

Yadan Quan and Huiyu Duan contributed equally to this work and share first authorship.

Y. Quan · Y. Shen · R. Lin · T. Liu · T. Zhang ·
J. Wu · X. Sun (✉)
Department of Ophthalmology and Visual Science,
Eye, Ear, Nose and Throat Hospital, Shanghai
Medical College, Fudan University, Shanghai
200031, China
e-mail: xhsun@shmu.edu.cn;

Y. Quan · R. Lin · T. Liu · T. Zhang · J. Wu · X. Sun
Shanghai Key Laboratory of Visual Impairment and
Restoration, Fudan University, Shanghai, China

Y. Quan · R. Lin · T. Liu · T. Zhang · J. Wu · X. Sun
NHC and Chinese Academy of Medical Sciences Key
Laboratory of Myopia, Fudan University, Shanghai,
China

H. Duan · J. Huang · G. Zhai
Institute of Image Communication and Network
Engineering, Shanghai Jiao Tong University,
Shanghai, China

Methods: Forty-six patients (mean age 41.00 ± 13.03 years) with POAG and 23 healthy controls (mean age 42.00 ± 11.08 years) were enrolled. All participants underwent sequenced PLR tests of full-field, superior/inferior quadrant-field chromatic stimuli using a binocular head-mounted pupillometer. The constricting amplitude, velocity, and time to max constriction/dilation, and the post-illumination pupil response (PIPR) were analyzed. The inner retina thickness and volume measurements were determined by spectral domain optical coherence tomography.

Z. Zhan
Shenzhen Eye Hospital, Shenzhen, China

X. Song · Y. Zhou
Department of Ophthalmology, Ninth People's
Hospital of Shanghai, Shanghai Jiao Tong University
School of Medicine, Shanghai, China

X. Sun
State Key Laboratory of Medical Neurobiology,
Institutes of Brain Science and Collaborative
Innovation Center for Brain Science, Fudan
University, Shanghai, China

Z. Zhan
Shenzhen Eye Institute, Shenzhen, China

Z. Zhan
Shenzhen Eye Hospital Affiliated to Jinan
University, Shenzhen, China

X. Song · Y. Zhou
Shanghai Key Laboratory of Orbital Diseases and
Ocular Oncology, Shanghai, China

Results: In the full-field stimulus experiment, time to pupil dilation was inversely correlated with perifoveal thickness ($r = -0.429$, $P < 0.001$) and perifoveal volume ($r = -0.364$, $P < 0.001$). Dilation time (AUC 0.833) showed good diagnostic performance, followed by the constriction amplitude (AUC 0.681) and PIPR (AUC 0.620). In the superior quadrant-field stimulus experiment, time of pupil dilation negatively correlated with inferior perifoveal thickness ($r = -0.451$, $P < 0.001$) and inferior perifoveal volume ($r = -0.417$, $P < 0.001$). The dilation time in response to the superior quadrant-field stimulus showed the best diagnostic performance (AUC 0.909). In the inferior quadrant-field stimulus experiment, time to pupil dilation ($P < 0.001$) correlated well with superior perifoveal thickness ($r = -0.299$, $P < 0.001$) and superior perifoveal volume ($r = -0.304$, $P < 0.001$).

Conclusion: The use of chromatic pupillometry offers a patient-friendly and objective approach to detect POAG, while the impairment of PLR features may serve as a potential indicator of structural macular damage.

Keywords: Chromatic pupillometry; Primary open-angle glaucoma; Macular structure

Key Summary Points

Why carry out this study?

Chromatic pupillometry presents high efficacy in the detection of pupillary light response (PLR) dysfunction in glaucoma.

The current study investigated the changes in PLR induced by full-field and quadrant-field stimuli in primary open-angle glaucoma (POAG), as well as examining the correlation between PLR features and macular measurements.

As far as we are aware, this is the first study to examine the correlation between PLR features and macular measurements.

What was learned from this study?

Our findings highlight the potential effectiveness of utilizing a head-mounted chromatic pupillometer as an objective method for detecting glaucomatous damage.

The observed impairment of PLR may signify concomitant structural macular damage, underscoring the diagnostic value of this approach.

INTRODUCTION

Glaucoma is one of the leading causes of irreversible blindness worldwide [1, 2]. The glaucomatous neuropathy is characterized by loss of retinal ganglion cells (RGCs), leading to the presence of structural hallmarks such as thinning of RGC-related retinal layers, and enlargement of the cup-to-disc ratio [2–4]. The most common form of glaucoma is primary open-angle glaucoma (POAG) with a prevalence of approximately 3.1% globally [2]. The current diagnostic tools for detecting glaucoma, such as optical coherence tomography (OCT) and standard automated perimetry (SAP), require expensive and highly calibrated equipment. However, SAP is subjective and time-consuming, and may not always reflect the glaucomatous structural changes [4]. The macular region contains more than half of all RGCs and it was previously believed that POAG spared this region until the late stage of the disease [5]. However, recent studies have shown that OCT measurements of macular thickness can provide a highly accurate diagnostic performance for detecting glaucoma, even in the early stage [6, 7].

Chromatic pupillometry is a quantitative and objective assessment that measures the pupil light response (PLR) to different wavelengths and irradiance of light stimulus, providing a means to evaluate the integrity of retinal and optic nerve health [8–11]. With advancements in instrumentation and analysis techniques, the precise quantification of PLR

features is now possible [12]. By employing various light wavelengths and irradiances, one can evaluate the overall integrity of PLR circuits driven by different retinal photoreceptor types, including rods, cones, and intrinsically photosensitive retinal ganglion cells (ipRGCs) [8, 11, 13, 14]. Rod and cone photoreceptors as well as ipRGCs differ in the properties of their response, thus providing an indication of the function of each cell type [11]. ipRGCs are a group of RGCs that transmit information to the suprachiasmatic nucleus (SCN) and the olivary pretectal nucleus (OPN), mediating non-image/image-forming vision, PLRs, and circadian photoentrainment [15–19]. Although ipRGCs constitute a small portion of total RGCs, several studies showed that ipRGC loss or dysfunction could be detected in patients with glaucoma [12, 20–27]. The shortened PLR constriction amplitude and sluggish post-illumination pupil response (PIPR) representing melanopsin dysfunction have been observed in patients with glaucoma [21–24, 26].

Although chromatic pupillometry presents promising results in the detection of PLR dysfunction in glaucoma, the situational constraints, interpretation of tests, and complexity of the devices make it challenging to implement in clinical or community-based settings. Little is known about the impact of glaucomatous macular damage, specifically macular RGC loss, on PLRs measured by chromatic pupillometry.

In this study, we aimed to explore whether the alterations in PLR features are related to glaucomatous RGC damage in the macular region, and to evaluate the feasibility of binocular chromatic pupillometer in opportunistic POAG diagnosis. The current study employed a head-mounted binocular pupillometer to investigate the changes in PLR features induced by full-field and quadrant-field stimuli in POAG. To the best of our knowledge, this is the first study that addresses the association between PLR characteristics and macular measurements in POAG.

METHODS

Participants

Forty-six patients with POAG (16 female, 30 male) and 23 visually healthy control subjects (12 female, 11 male) participated. Glaucoma participants were recruited from the Eye and ENT Hospital of Fudan University (Shanghai, China). The research followed the tenets of the Declaration of Helsinki, and the study was approved by the human subjects review committee of the Eye and ENT Hospital of Fudan University. Written informed consent was obtained from each participant. All subjects received PLR tests on a headset (Fig. 1) and comprehensive ophthalmologic examinations including intraocular pressure measurement, slit-lamp stereo biomicroscopy, direct ophthalmoscopy, OCT, and SAP. Subjects with retinopathies, other causes of optic neuropathy, or ocular motor disorders were excluded from the study. Subjects with diabetes, psychiatric or neurologic disorders, including cognitive impairment or dementia, as well as those who had previously undergone intraocular surgery or were taking psychotropic or other medications that could potentially affect the PLR or alertness were also excluded.

SAP Tests

SAP was evaluated with the Octopus 900 perimeter to test the visual field (VF) (Haag-Streit, Koeniz, Switzerland), G standard white/white TOP program. All SAP tests were required to meet reliability criteria. VF tests were defined as abnormal when they met one of the following conditions: (1) the presence of three or more adjacent points in the superior or inferior field with $P < 5\%$ probability of normal range and one or more points with $P < 1\%$ probability of normal range; (2) presence of two or more adjacent points with $P < 1\%$ probability of normal range and one or more points with

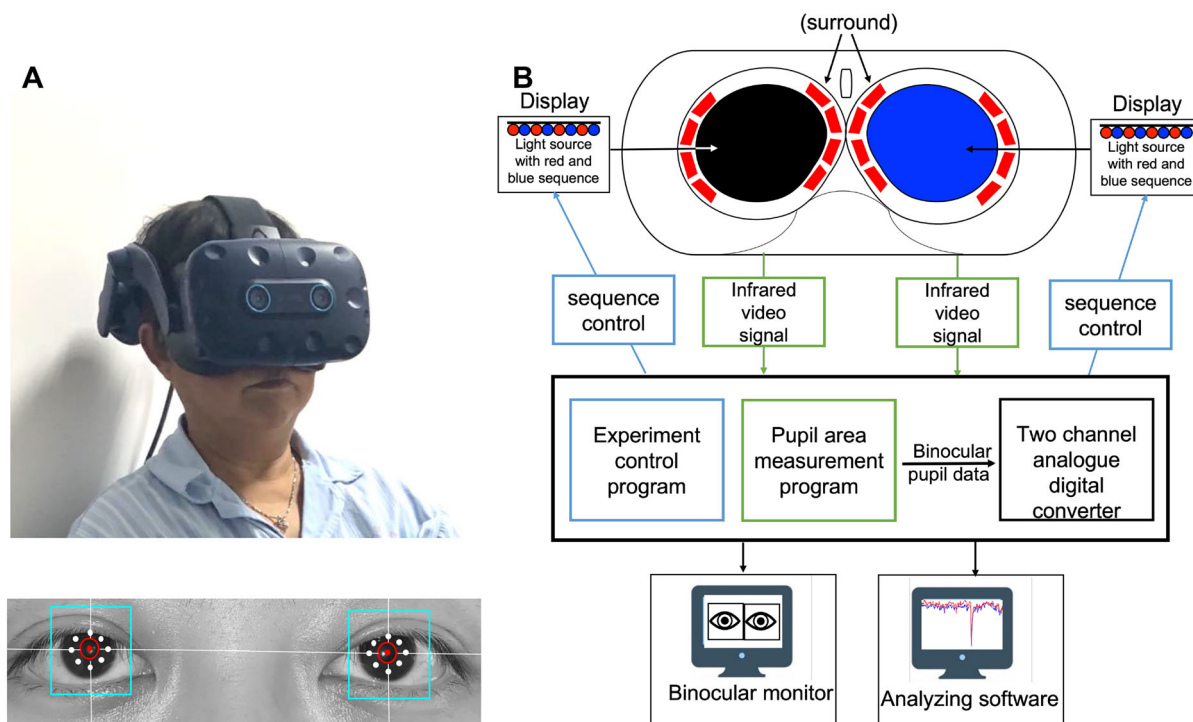


Fig. 1 **a** Subject underwent the PLR test on a headset, and the PLR curve was recorded by the surrounding IR cameras. **b** Scheme of the binocular chromatic pupillometer

$P < 2\%$ probability. Patients with POAG were further divided into mild–moderate stage (mean deviation (MD) scores < 12 dB) and severe-stage (MD scores ≥ 12 dB) groups according to Hodapp–Parrish–Anderson criteria [28].

OCT Examinations

Optical coherence tomography was performed with spectral domain optical coherence tomography OCT (Optovue, Inc., Fremont, CA, USA). All OCT scans were obtained using the MM5 protocol consisting of a 5 mm by 5 mm grid of horizontal and vertical scans through the macula, and a standard ganglion cell complex (GCC) scan. The inner retina was defined as the retinal nerve fiber layer, ganglion cell layer, and inner plexiform layer. Thickness and volume data were generated by the Optovue software and were recorded from thickness maps (Fig. 2c–f). The measurement regions and inner retinal segmentation boundaries are illustrated in Fig. 2c, d. For thickness and

volume measurements, evaluated regions include the superior hemisphere, and inferior hemisphere areas of the parafoveal and perifoveal regions, as well as the central foveal zone [29].

Apparatus and Calibration of Binocular Pupillometer

The pupillometer setup consists of an HTC Vive Pro, with an integrated eye tracker (Tobii pro, Tobii Technology, Stockholm, Sweden). The visual stimuli are generated in Unity 2018, utilizes SteamVR 2.0, and runs on a laptop computer (MEHREV Z2, NVIDIA GeForce GTX 2060 i7-10870H@2.20 GHz, 16 GB RAM). Subjects were fitted with helmet-mounted displays (HMDs), using near-infrared (940 nm) illuminating diodes and infrared cameras to track pupillary data (sample rate 90 Hz). Both eyes were tested in turn. Stimulus wavelength and luminance were verified with a

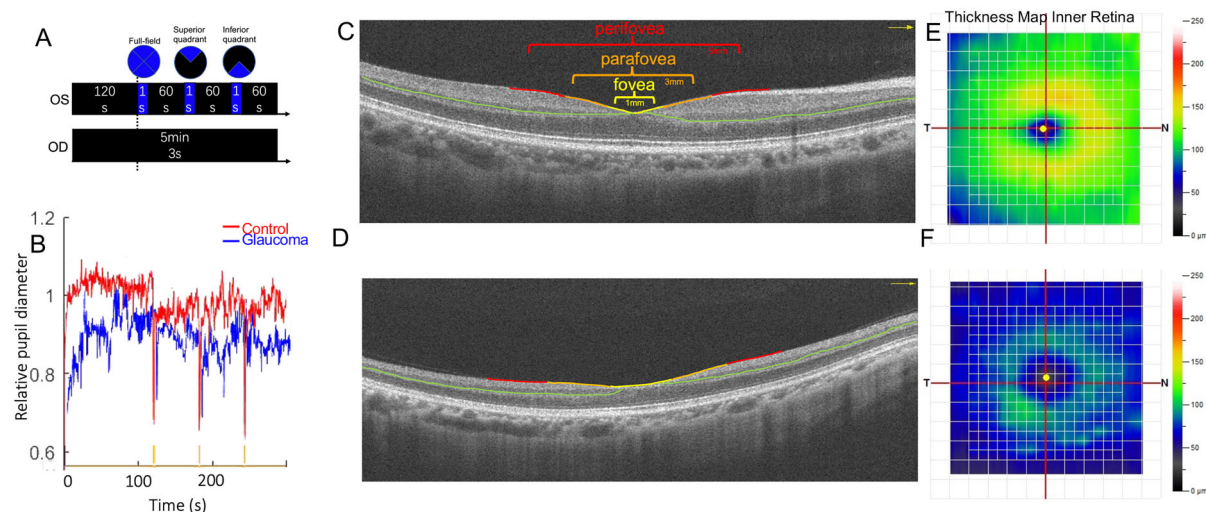


Fig. 2 **a** Chromatic pupillometry protocol of sequenced PLR tests. **b** PLR curve of one healthy eye (red line) and a glaucomatous eye (blue line). Representative optical coherence tomography macular scan used for thickness and volume measurements of a healthy control (**c**) and in a patient with POAG (**d**). The green line represents the

boundaries of the inner retina. The fovea (yellow), parafovea (orange), and perifovea (red) regions are denoted. Representative thickness map of macular regions used for thickness and volume measurements in a healthy control (**e**) and in a patient with POAG (**f**). More green color represents a thinner inner retina

spectroradiometer (Konica CS-100A; Konica Minolta, Inc., Tokyo, Japan).

Stimuli and Procedures

After calibration of HMDs, dark adaption was performed by displaying a dark screen for 120 s. Full-field (110° in diameter) of short-wavelength (“blue” dominant wavelength of 465 nm, luminance of 100 cd/m^2) pulses of light were shone for 1 s after dark adaption. After 60 s rest, the superior and inferior quadrant flash stimuli were presented in turn (Fig. 2a). The pupillary response curve was recorded (Fig. 2b).

Data Acquisition and Feature Extraction

During the experiment, real-time pupil diameter was recorded (90 Hz). Data were analyzed offline using custom scripts programmed in MATLAB (MathWorks, Inc., Natick, MA, USA), which automated interpolated eye movement and filtered short-time (< 500 ms) eye blinks.

The following components were extracted in three experiments:

Baseline pupil diameter (BPD) (mm): mean pupillary diameter during the initial 10 s before light onset.

Maximum constriction amplitude (%) = $\frac{\text{BPD} - \text{maximum constriction pupil diameter}}{\text{BPD}} \times 100\%$.

Time to maximum constriction (s): the interval between the beginning stimulus and peak constriction.

Time to pupil dilation (s): the interval between the beginning of light stimulus and the pupil diameter recovered to 90% BPD.

Constriction velocity (mm/s): $\frac{\text{BPD} - \text{maximum constriction pupil diameter (mm)}}{\text{time to maximal constriction (s)}}$.

Dilation velocity (mm/s): $\frac{\text{BPD} - \text{maximum constriction pupil diameter (mm)}}{\text{time to dilation (s)}}$.

Sustained response (mm): the pupil diameter at 6 s after the flashlight offset.

PIPR: $\frac{\text{BPD} - \text{PD at 6 s after flash offset}}{\text{BPD}} \times 100\%$.

Table 1 Ocular characteristics of the study eyes in the control and glaucoma groups

	Healthy control	Glaucoma	Mild–moderate glaucoma	P value			
				Control vs glaucoma	Control vs mild–moderate glaucoma	Control vs severe glaucoma	Mild–moderate glaucoma vs severe glaucoma
N	46	92	72	NA	NA	NA	NA
Age (mean ± SD) (years)	42.00 (11.08)	41.00 (13.03)	39.61 (11.65)	NA	NA	NA	NA
MD, median (IQR) (dB)	2.45 (1.40, 3.08)	5.65 (3.00, 9.35)	4.49 (2.50, 6.80)	< 0.001	< 0.001	< 0.001	< 0.001
Macular thickness (IQR) (μm)	64.00 (59.00, 70.00)	64.50 (57.00, 73.25)	64.50 (57.75, 73.00)	0.445	NA	NA	NA
Macular volume (IQR) (mm ³)	0.05 (0.04, 0.06)	0.05 (0.05, 0.06)	0.05 (0.05, 0.06)	0.276	NA	NA	NA
Parafoveal thickness (IQR) (μm)	122.00 (116.00, 127.00)	117.00 (102.00, 123.00)	119.00 (109.75, 123.25)	0.002	0.055	< 0.001	0.001
Parafoveal volume (IQR) (mm ³)	0.77 (0.73, 0.80)	0.74 (0.64, 0.77)	0.75 (0.69, 0.78)	0.002	0.061	< 0.001	0.001
Perifoveal thickness (IQR) (μm)	108.00 (105.00, 111.00)	96.50 (88.00, 104.00)	100.00 (92.75, 105.00)	< 0.001	< 0.001	< 0.001	< 0.001
Perifoveal volume (IQR) (mm ³)	1.35 (1.29, 1.39)	1.20 (1.10, 1.30)	1.25 (1.15, 1.32)	< 0.001	< 0.001	< 0.001	< 0.001
Inferior hemisphere GCC (IQR) (μm)	95.00 (91.25, 97.00)	77.00 (62.00, 85.25)	78.00 (71.00, 88.00)	< 0.001	< 0.001	< 0.001	< 0.001

Table 1 continued

	Healthy control	Glaucoma	Mild–moderate glaucoma	P value			
				Control vs glaucoma	Control vs mild–moderate glaucoma	Control vs severe glaucoma	Mild–moderate glaucoma vs severe glaucoma
Inner retina parafoveal inferior hemisphere thickness (IQR) (μm)	120.00 (115.00, 126.00)	114.50 (101.75, 121.25)	117.00 (106.75, 122.00)	0.001	0.038	< 0.001	0.002
Inner retina parafoveal inferior hemisphere volume (IQR) (mm ³)	0.38 (0.36, 0.40)	0.36 (0.32, 0.38)	0.37 (0.33, 0.38)	< 0.001	0.007	< 0.001	0.002
Inner retina perifoveal inferior hemisphere thickness (IQR) (μm)	107.50 (102.25, 110.75)	93.00 (83.00, 100.25)	96.00 (88.75, 103.00)	< 0.001	< 0.001	< 0.001	< 0.001
Inner retina perifoveal inferior hemisphere volume (IQR) (mm ³)	0.68 (0.64, 0.69)	0.59 (0.52, 0.64)	0.61 (0.56, 0.65)	< 0.001	< 0.001	< 0.001	< 0.001
Superior hemisphere GCC (IQR) (μm)	95.00 (92.00, 98.00)	85.00 (68.00, 93.00)	87.00 (76.00, 95.25)	< 0.001	< 0.001	< 0.001	< 0.001
Inner retina parafoveal superior hemisphere thickness (IQR)(μm)	122.50 (117.00, 126.00)	118.00 (101.00, 125.25)	121.00 (109.00, 127.50)	0.032	0.301	< 0.001	0.001
Inner retina parafoveal superior hemisphere volume (IQR)(mm ³)	0.38 (0.37, 0.40)	0.37 (0.32, 0.39)	0.38 (0.34, 0.40)	0.021	0.213	< 0.001	0.002
Inner retina perifoveal superior hemisphere thickness (IQR)(μm)	109.00 (105.00, 111.00)	100.50 (89.00, 108.00)	104.00 (95.00, 112.25)	< 0.001	0.004	< 0.001	< 0.001

Table 1 continued

	Healthy control	Glaucoma	Mild–moderate glaucoma	P value			
				Control vs glaucoma	Control vs mild–moderate glaucoma	Control vs severe glaucoma	Mild–moderate glaucoma vs severe glaucoma
Inner retina perifoveal superior hemisphere volume (IQR) (mm ³)	0.68 (0.66, 0.70)	0.63 (0.56, 0.69)	0.65 (0.60, 0.71)	0.001	0.035	< 0.001	< 0.001

A Kruskal–Wallis one-way ANOVA on ranks was used to compare controls, mild–moderate stage, and severe stage glaucoma groups. A post hoc pairwise comparison between the three groups was done using Dunn's method. Comparison between two groups was evaluated by using the Wilcoxon rank-sum test IQR interquartile range, MD mean deviation, GCC ganglion cell complex, NA not applicable.

Statistical Analysis

Ophthalmologic examination outcomes and pupillometric features are represented as means \pm standard deviation or median (interquartile range). Comparisons between healthy controls and the different glaucoma severity groups were evaluated by using one-way analysis of variance (ANOVA) or Kruskal–Wallis one-way analysis of variance on ranks test. Post hoc analysis (LSD) or Dunn's method was further performed to identify significant group differences. One-way ANOVA or the Wilcoxon rank-sum test was used to compare pairs of groups (Table 1). The correlation between pupillometric features and macular measures or MD score was assessed using Spearman's rank correlation. A receiver operating characteristic curve (ROC) and the area under the ROC curve (AUC) analysis was calculated to compare the diagnostic value using the pROC package and reportROC package. The sensitivity, specificity, and 95% CI were calculated at the best statistical cutoff. Comparison between the AUCs of pupillometric features and macular structures was performed using DeLong's method with Bonferroni correction. The threshold for significance for all statistical tests was set at 0.05. Statistical procedures were performed using R version 4.2.2 (R: a language and environment for statistical computing, R Core Team, Vienna, Austria).

RESULTS

Of the 138 eligible eyes included in this study, 46 were assigned to the healthy control group and 92 were assigned to the glaucoma group: 72 eyes to the mild–moderate glaucoma group, and 20 to the severe glaucoma group. No significant differences in age and gender were found between the control group and the glaucoma group or among different staged glaucoma groups. The mean age of control subjects was 42.00 ± 11.08 years old, and the mean age of the glaucoma group was 41.00 ± 13.03 years old. There was no statistical difference in age distribution between the patients with glaucoma and healthy controls.

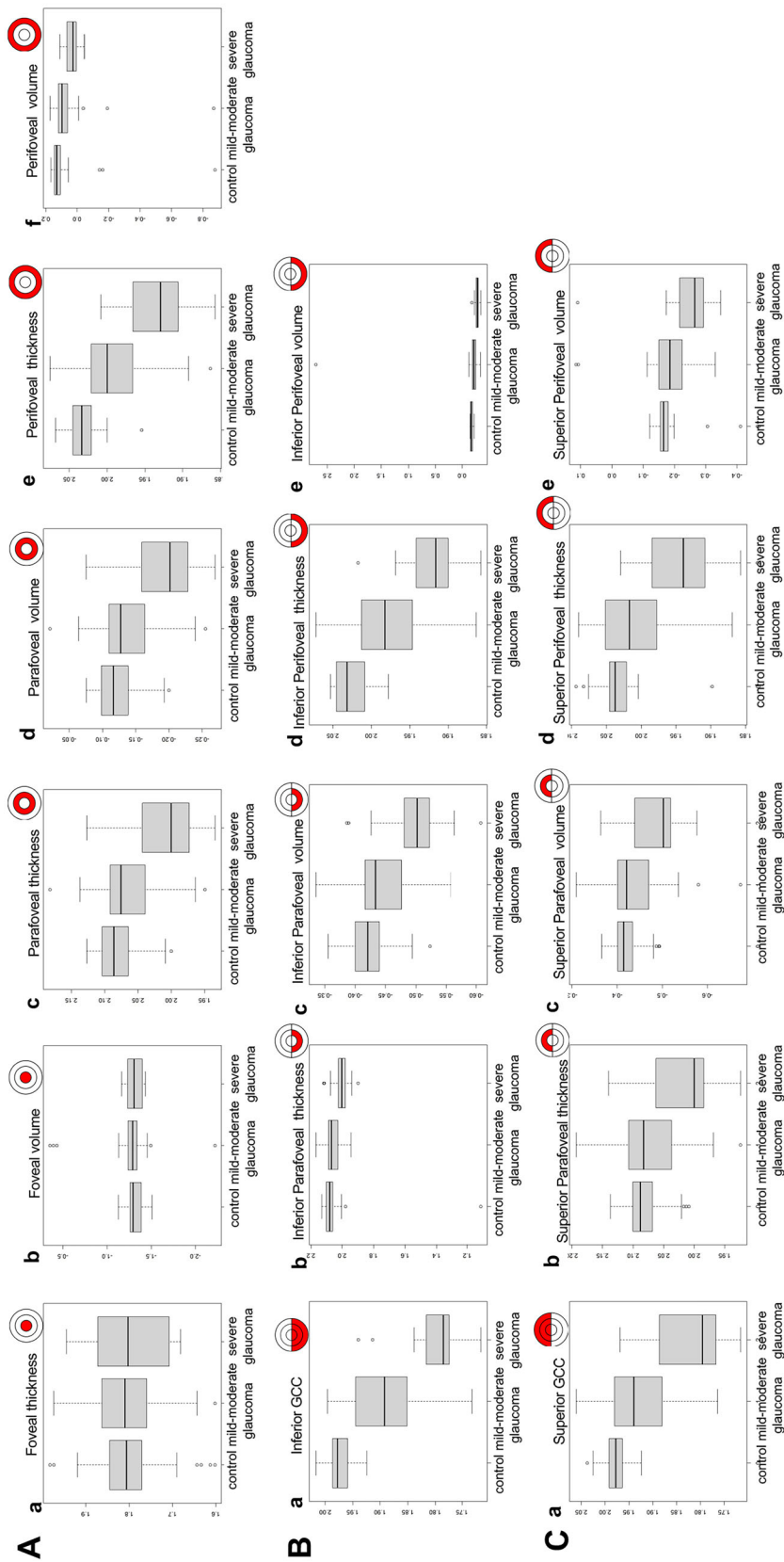


Fig. 3 Macular measurements comparisons between control, mild-moderate glaucoma, and severe glaucoma. **A (a-f)** Central macular measurements. **B (a-e)** Inferior hemisphere of the macular region. Y-axis shows the log value of measurements

Table 2 Pupillometric features of the study eyes in the control and glaucoma groups

	Healthy control	Glaucoma	Mild–moderate glaucoma	Severe glaucoma	<i>P</i>		
					Control vs glaucoma	Control vs mild–moderate glaucoma	Control vs severe glaucoma vs mild–moderate glaucoma
<i>N</i>	46	92	72	20	NA	NA	NA
Amplitude full-field (IQR)	0.43 ± 0.07	0.39 ± 0.07	0.39 ± 0.08	0.38 ± 0.05	0.001	0.003	0.006
Sustained response full-field (IQR) (mm)	5.43 (4.85, 6.11)	5.25 (4.67, 5.93)	5.28 (4.70, 6.00)	5.01 (4.49, 5.61)	0.162	NA	NA
PIPR full-field (IQR)	0.09 (0.06, 0.11)	0.12 (0.06, 0.16)	0.11 (0.06, 0.15)	0.13 (0.11, 0.17)	0.015	0.116	0.007
T constriction full-field (IQR) (s)	1.46 (1.38, 1.53)	1.44 (1.31, 1.53)	1.44 (1.32, 1.52)	1.47 (1.30, 1.57)	0.299	NA	NA
T dilation full-field (IQR) (s)	15.64 (12.48, 16.68)	17.28 (16.67, 17.65)	17.17 (16.33, 17.53)	17.72 (17.20, 18.62)	< 0.001	< 0.001	< 0.001
Vel constriction full-field (IQR) (mm/s)	1.75 ± 0.29	1.68 ± 0.40	1.69 ± 0.43	1.62 ± 0.28	0.289	NA	NA
Vel dilation full-field (IQR) (mm/s)	0.16 (0.15, 0.20)	0.17 (0.14, 0.21)	0.17 (0.14, 0.21)	0.15 (0.13, 0.21)	0.987	NA	NA
Amplitude superior quadrant-field (IQR)	0.61 (0.55, 0.68)	0.65 (0.60, 0.71)	0.65 (0.61, 0.71)	0.66 (0.58, 0.76)	0.007	0.019	0.321
Sustained response superior quadrant-field (IQR) (mm)	5.51 ± 0.91	5.30 ± 0.88	5.38 ± 0.85	5.01 ± 0.96	0.197	NA	NA
PIPR superior quadrant-field (IQR)	0.08 (0.02, 0.14)	0.10 (0.06, 0.17)	0.10 (0.05, 0.15)	0.16 (0.08, 0.22)	0.101	0.356	0.018

Table 2 continued

	Healthy control	Glaucoma	Mild–moderate glaucoma	Severe glaucoma	<i>P</i>			
					Control vs glaucoma	Control vs mild–moderate glaucoma	Control vs severe glaucoma	Mild–moderate glaucoma vs severe glaucoma
T constriction superior quadrant-field (IQR) (s)	1.35 (1.24, 1.41)	1.27 (1.08, 1.39)	1.27 (1.10, 1.39)	1.25 (1.07, 1.42)	0.035	NA	NA	NA
T dilation superior quadrant-field (IQR) (s)	16.04 (14.41, 16.74)	17.73 (17.15, 18.22)	17.63 (17.09, 18.06)	17.90 (17.49, 19.41)	< 0.001	< 0.001	< 0.001	0.040
Vel constriction superior quadrant-field (IQR) (mm/s)	1.75 ± 0.38	1.66 ± 0.37	1.67 ± 0.36	1.61 ± 0.40	0.157	NA	NA	NA
Vel dilation superior quadrant-field (IQR) (mm/s)	0.15 (0.13, 0.18)	0.14 (0.11, 0.23)	0.15 (0.12, 0.24)	0.12 (0.10, 0.17)	0.621	NA	NA	NA
Amplitude inferior quadrant-field (IQR)	0.60 ± 0.08	0.64 ± 0.10	0.64 ± 0.10	0.64 ± 0.10	0.028	NA	NA	NA
Sustained response inferior quadrant-field (IQR) (mm)	5.48 ± 0.94	5.22 ± 0.83	5.27 ± 0.81	5.06 ± 0.89	0.103	NA	NA	NA
PIPR inferior quadrant-field (IQR)	0.09 ± 0.10	0.12 ± 0.08	0.12 ± 0.09	0.14 ± 0.07	0.061	0.143	0.035	0.249
T constriction inferior quadrant-field (IQR) (s)	1.38 (1.27, 1.45)	1.37 (1.29, 1.44)	1.37 (1.31, 1.44)	1.34 (1.20, 1.41)	0.743	NA	NA	NA
T dilation inferior quadrant-field (IQR) (s)	16.07 (13.11, 16.78)	17.53 (16.61, 17.97)	17.28 (16.40, 17.81)	18.18 (17.50, 19.19)	< 0.001	< 0.001	< 0.001	0.001

Table 2 continued

	Healthy control	Glaucoma	Mild–moderate glaucoma	Severe glaucoma	<i>P</i>			
					Control vs glaucoma	Control vs mild–moderate glaucoma	Control vs severe glaucoma vs mild–moderate glaucoma	
Vel constriction inferior quadrant-field (IQR) (mm/s)	1.76 ± 0.35	1.58 ± 0.42	1.58 ± 0.42	1.59 ± 0.41	0.011	0.014	0.109	0.876
Vel dilation inferior quadrant-field (IQR) (mm/s)	0.16 (0.13, 0.19)	0.15 (0.12, 0.20)	0.15 (0.13, 0.22)	0.15 (0.12, 0.17)	0.696	NA	NA	NA

A Kruskal–Wallis one-way ANOVA on ranks was used to compare controls, mild–moderate stage, and severe stage glaucoma groups. A post hoc pairwise comparison between the three groups was done using Dunn’s method. Comparison between two groups was evaluated by using the Wilcoxon rank-sum test (IQR interquartile range, PIPR post-illumination pupil response, *T* time, *Vel* velocity, NA not applicable).

Macular Structural Features

Figure 2c, d illustrates the macular measurements for cases and controls. Figure 2e, f depicts the thickness maps of the inner retina. Table 1 and Fig. 3 summarize the macular thickness and volume measurements. The thickness ($P = 0.445$) and volume ($P = 0.276$) measurements of the fovea did not differ between the control and the glaucoma group. Most inner retinal measurements, namely parafoveal thickness, parafoveal volume, perifoveal thickness, and perifoveal volume, were reduced in glaucoma groups (Fig. 3A). The macular measurements in both hemispheres in the perifoveal and parafoveal areas were decreased in the glaucoma groups (Fig. 3B, C). The most discriminating parameter was the thickness of the inner retina perifoveal inferior hemisphere (13.5% decline in glaucoma), followed by the volume of the inner retina perifoveal inferior hemisphere (13.2% decline in glaucoma).

Pupillometric Features

Figure 2b presents the PLR curves of a control subject (red) and a patient with glaucoma (blue) while being exposed in sequence to a full-field stimulus, a superior quadrant-field stimulus, and an inferior quadrant-field stimulus. The PLR curve presents as a transient constriction response followed by a dilation to baseline in response to three stimuli. The subject age or gender does not have a significant impact on pupillometric features.

Table 2 summarizes the pupillometric features of healthy controls and patients with different stages of glaucoma. In response to the full-field stimulus, the constriction amplitude was greater in controls compared to patients with glaucoma ($P = 0.001$), but there was no significance between groups with different stages of glaucoma ($P = 0.506$). The PIPR was decreased in the glaucoma group compared to the control group ($P = 0.015$), but no significant difference between groups with different stages of glaucoma was observed ($P = 0.116$). The time to pupil dilation was significantly prolonged in glaucoma groups ($P < 0.001$), and significantly

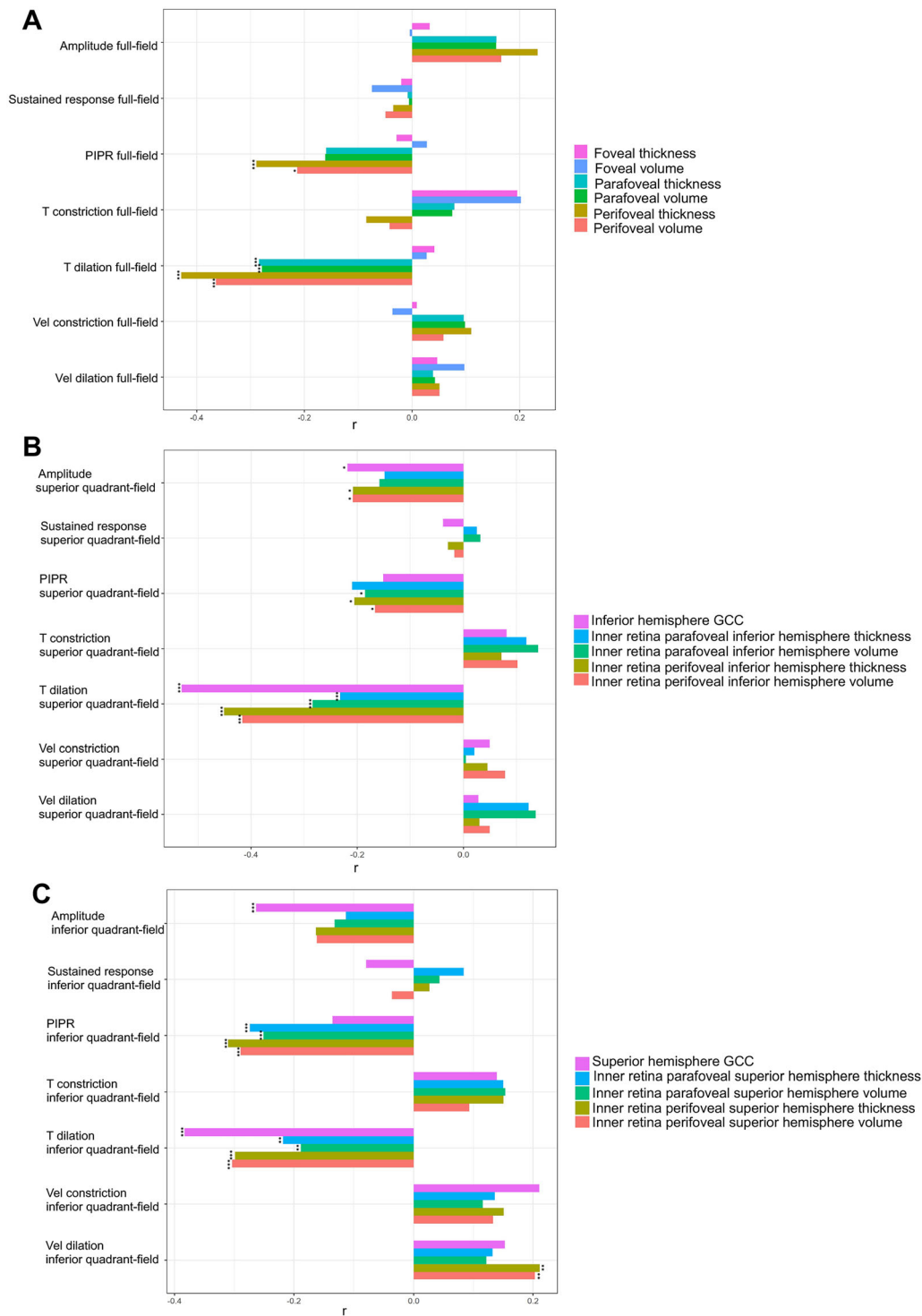


Fig. 4 Correlations of PLR features and macular structural measurements in full-field stimulus (a), superior quadrant-field stimulus (b), and inferior quadrant-field stimulus (c). X-axis shows the Spearman’s correlation

coefficient. Symbols denote regions that are statistically significant between the cases and controls (* $P < 0.05$, ** $P < 0.01$, *** $P < 0.001$). *T* time, *Vel* velocity, *PIPR* post-illumination pupil response

Table 3 Spearman's rank correlations for pupillometric features and vision field median deviation

Variable	Spearman's rank correlation	<i>P</i> value
Amplitude full-field	− 0.372	< 0.001
Sustained response full-field	− 0.154	0.070
PIPR full-field	0.280	< 0.001
T constriction full-field	− 0.035	0.688
T dilation full-field	0.479	< 0.001
Vel constriction full-field	− 0.293	< 0.001
Vel dilation full-field	− 0.225	0.008
Amplitude superior quadrant-field	0.225	0.108
Sustained response superior quadrant-field	− 0.117	0.173
PIPR superior quadrant-field	0.184	0.030
T constriction superior quadrant-field	− 0.106	0.215
T dilation superior quadrant-field	0.502	< 0.001
Vel constriction superior quadrant-field	− 0.143	0.093
Vel dilation superior quadrant-field	− 0.205	0.016
Amplitude inferior quadrant-field	0.180	0.134
Sustained response inferior quadrant-field	− 0.081	0.346
PIPR inferior quadrant-field	0.108	0.206
T constriction inferior quadrant-field	− 0.135	0.116
T dilation inferior quadrant-field	0.515	< 0.001
Vel constriction inferior quadrant-field	− 0.177	0.037

Table 3 continued

Variable	Spearman's rank correlation	<i>P</i> value
Vel dilation inferior quadrant-field	− 0.238	0.005

IQR interquartile range, *PIPR* post-illumination pupil response, *T* time, *Vel* velocity

different between the two glaucoma groups ($P = 0.002$). The constriction-related variables did not differ between controls and patients with glaucoma.

In response to the superior quadrant-field stimulus, the most distinguishable PLR feature was the time to pupil dilation ($P < 0.001$). The constriction amplitude was greater in controls compared to patients with glaucoma ($P = 0.007$), and the time to maximum constriction was faster in controls compared to patients with glaucoma ($P = 0.035$). The PIPR to superior quadrant-field stimulus was decreased in the severe glaucoma group compared to the control group ($P = 0.018$).

In response to the inferior quadrant-field stimulus, the most distinguishable PLR feature was the time to pupil dilation ($P < 0.001$). The PIPR to inferior quadrant-field stimulus was significantly decreased in the severe glaucoma group compared to the control group ($P = 0.035$). Additionally, the velocity of constriction was also reduced in the glaucoma group ($P = 0.011$).

Correlation of Pupillometric Features and Ocular Characteristics

Spearman's correlation coefficients were calculated to assess the relationship between pupillometric features and macular measurements (Fig. 4). In the full-field stimulus experiment, the time to pupil dilation was inversely correlated with the parafoveal thickness ($r = -0.284$, $P < 0.001$), the parafoveal volume ($r = -0.279$, $P < 0.001$), the perifoveal thickness ($r = -0.429$, $P < 0.001$), and the perifoveal volume ($r = -0.364$, $P < 0.001$). The PIPR to full-field stimulus was negatively correlated

Table 4 Diagnostic value of pupillometric parameters

	Control vs glaucoma			Control vs mild-moderate glaucoma			Control vs severe glaucoma			Mild-moderate glaucoma vs severe glaucoma		
	AUC	Sensitivity	Specificity	AUC	Sensitivity	Specificity	AUC	Sensitivity	Specificity	AUC	Sensitivity	Specificity
Amplitude full-field	0.681 (0.583, 0.778)	0.598 (0.498, 0.698)	0.761 (0.638, 0.884)	0.665 (0.563, 0.766)	0.569 (0.455, 0.684)	0.783 (0.663, 0.902)	0.739 (0.614, 0.865)	0.800 (0.625, 0.975)	0.674 (0.538, 0.809)	0.535 (0.405, 0.665)	0.850 (0.694, 1.000)	0.375 (0.263, 0.487)
Sustained response full-field	0.573 (0.473, 0.674)	0.185 (0.105, 0.264)	0.978 (0.936, 1.000)	0.550 (0.444, 0.656)	0.153 (0.070, 0.236)	1.000 (1.000, 1.000)	0.657 (0.516, 0.797)	1.000 (1.000, 1.000)	0.261 (0.134, 0.388)	0.587 (0.456, 0.718)	0.950 (0.854, 1.000)	0.306 (0.199, 0.412)
PIPR full-field	0.627 (0.535, 0.719)	0.554 (0.453, 0.656)	0.739 (0.612, 0.866)	0.590 (0.488, 0.692)	0.333 (0.224, 0.442)	0.935 (0.863, 1.000)	0.762 (0.625, 0.899)	0.700 (0.499, 0.901)	0.739 (0.612, 0.866)	0.622 (0.489, 0.755)	0.900 (0.769, 1.000)	0.403 (0.289, 0.516)
T constriction full-field	0.554 (0.458, 0.651)	0.283 (0.191, 0.375)	0.935 (0.863, 1.000)	0.563 (0.459, 0.667)	0.278 (0.174, 0.381)	0.935 (0.863, 1.000)	0.523 (0.344, 0.702)	0.300 (0.099, 0.501)	0.957 (0.898, 1.000)	0.522 (0.358, 0.686)	0.250 (0.060, 0.440)	0.958 (0.912, 1.000)
T dilation full-field	0.833 (0.764, 0.902)	0.739 (0.649, 0.829)	0.761 (0.638, 0.884)	0.800 (0.720, 0.880)	0.875 (0.799, 0.951)	0.565 (0.422, 0.708)	0.950 (0.904, 0.996)	1.000 (1.000, 1.000)	0.826 (0.717, 0.936)	0.765 (0.653, 0.877)	1.000 (1.000, 1.000)	0.458 (0.343, 0.573)
Vel constriction full-field	0.556 (0.459, 0.652)	0.500 (0.398, 0.602)	0.674 (0.538, 0.809)	0.538 (0.435, 0.642)	0.333 (0.224, 0.442)	0.870 (0.772, 0.967)	0.618 (0.469, 0.768)	0.650 (0.441, 0.859)	0.652 (0.515, 0.790)	0.540 (0.413, 0.667)	0.700 (0.499, 0.901)	0.500 (0.385, 0.615)
Vel dilation full-field	0.501 (0.401, 0.601)	0.315 (0.220, 0.410)	0.783 (0.663, 0.902)	0.514 (0.407, 0.620)	0.542 (0.427, 0.657)	0.587 (0.445, 0.729)	0.553 (0.383, 0.723)	0.350 (0.141, 0.559)	0.848 (0.744, 0.952)	0.558 (0.406, 0.710)	0.550 (0.332, 0.768)	0.681 (0.573, 0.788)
Amplitude superior quadrant-field	0.641 (0.541, 0.740)	0.815 (0.736, 0.895)	0.435 (0.292, 0.578)	0.651 (0.547, 0.756)	0.819 (0.731, 0.908)	0.478 (0.334, 0.623)	0.602 (0.440, 0.764)	0.300 (0.099, 0.501)	0.978 (0.936, 1.000)	0.536 (0.369, 0.703)	0.450 (0.232, 0.668)	0.819 (0.731, 0.908)
Sustained response superior quadrant-field	0.558 (0.457, 0.659)	0.587 (0.486, 0.688)	0.565 (0.422, 0.708)	0.530 (0.422, 0.638)	0.569 (0.455, 0.684)	0.565 (0.422, 0.708)	0.658 (0.502, 0.813)	0.350 (0.141, 0.559)	0.957 (0.898, 1.000)	0.622 (0.471, 0.772)	0.450 (0.232, 0.668)	0.847 (0.764, 0.930)
PIPR superior quadrant-field	0.586 (0.478, 0.694)	0.891 (0.828, 0.955)	0.304 (0.171, 0.437)	0.556 (0.444, 0.669)	0.875 (0.799, 0.951)	0.304 (0.171, 0.437)	0.692 (0.560, 0.825)	0.600 (0.385, 0.815)	0.783 (0.663, 0.902)	0.677 (0.537, 0.817)	0.600 (0.385, 0.815)	0.778 (0.682, 0.874)

Table 4 continued

	Control vs glaucoma			Control vs mild–moderate glaucoma			Control vs severe glaucoma			Mild–moderate glaucoma vs severe glaucoma		
	AUC	Sensitivity	Specificity	AUC	Sensitivity	Specificity	AUC	Sensitivity	Specificity	AUC	Sensitivity	Specificity
T constriction superior quadrant-field	0.611 (0.515, 0.706)	0.446 (0.344, 0.547)	0.848 (0.744, 0.952)	0.618 (0.517, 0.720)	0.444 (0.330, 0.559)	0.848 (0.744, 0.952)	0.583 (0.404, 0.761)	0.450 (0.232, 0.668)	0.891 (0.801, 0.981)	0.518 (0.358, 0.679)	0.250 (0.060, 0.440)	0.917 (0.853, 0.981)
T dilation superior quadrant-field	0.909 (0.855, 0.963)	0.837 (0.761, 0.912)	0.935 (0.863, 1.000)	0.892 (0.830, 0.953)	0.792 (0.698, 0.885)	0.935 (0.863, 1.000)	0.973 (0.939, 1.000)	1.000 (1.000, 1.000)	0.935 (0.863, 1.000)	0.685 (0.548, 0.822)	0.450 (0.232, 0.668)	0.889 (0.816, 0.961)
Vel constriction superior quadrant-field	0.553 (0.449, 0.657)	0.913 (0.855, 0.971)	0.239 (0.116, 0.362)	0.545 (0.436, 0.654)	0.875 (0.799, 0.951)	0.283 (0.152, 0.413)	0.582 (0.427, 0.736)	0.300 (0.099, 0.501)	0.935 (0.863, 1.000)	0.537 (0.381, 0.692)	0.300 (0.099, 0.501)	0.875 (0.799, 0.951)
Vel dilation superior quadrant-field	0.526 (0.431, 0.621)	0.272 (0.181, 0.363)	0.935 (0.863, 1.000)	0.505 (0.402, 0.609)	0.208 (0.115, 0.302)	0.978 (0.936, 1.000)	0.639 (0.463, 0.816)	0.500 (0.281, 0.719)	0.891 (0.801, 0.981)	0.602 (0.461, 0.743)	0.600 (0.385, 0.815)	0.667 (0.558, 0.776)
Amplitude inferior quadrant-field	0.610 (0.512, 0.707)	0.348 (0.251, 0.445)	0.870 (0.772, 0.967)	0.614 (0.511, 0.717)	0.333 (0.224, 0.442)	0.870 (0.772, 0.967)	0.593 (0.431, 0.756)	0.400 (0.185, 0.615)	0.870 (0.772, 0.967)	0.505 (0.347, 0.662)	0.350 (0.141, 0.559)	0.792 (0.698, 0.885)
Sustained response inferior quadrant-field	0.567 (0.464, 0.670)	0.641 (0.543, 0.739)	0.522 (0.377, 0.666)	0.549 (0.440, 0.657)	0.625 (0.513, 0.737)	0.522 (0.377, 0.666)	0.633 (0.483, 0.782)	0.400 (0.185, 0.615)	0.870 (0.772, 0.967)	0.591 (0.442, 0.740)	0.400 (0.185, 0.615)	0.833 (0.747, 0.919)
PIPR inferior quadrant-field	0.597 (0.492, 0.701)	0.859 (0.788, 0.930)	0.391 (0.250, 0.532)	0.575 (0.466, 0.685)	0.833 (0.747, 0.919)	0.391 (0.250, 0.532)	0.673 (0.539, 0.807)	0.950 (0.854, 1.000)	0.391 (0.250, 0.532)	0.607 (0.472, 0.742)	0.750 (0.560, 0.940)	0.514 (0.398, 0.629)
T constriction inferior quadrant-field	0.517 (0.411, 0.623)	0.620 (0.520, 0.719)	0.500 (0.356, 0.644)	0.506 (0.395, 0.617)	0.611 (0.499, 0.724)	0.500 (0.356, 0.644)	0.559 (0.403, 0.715)	0.800 (0.625, 0.975)	0.413 (0.271, 0.555)	0.560 (0.402, 0.717)	0.250 (0.060, 0.440)	0.931 (0.872, 0.989)
T dilation inferior quadrant-field	0.821 (0.750, 0.892)	0.696 (0.602, 0.790)	0.804 (0.690, 0.919)	0.784 (0.701, 0.867)	0.625 (0.513, 0.737)	0.804 (0.690, 0.919)	0.953 (0.908, 0.998)	0.950 (0.854, 1.000)	0.826 (0.717, 0.936)	0.777 (0.666, 0.888)	0.700 (0.499, 0.901)	0.792 (0.698, 0.885)

Table 4 continued

	Control vs glaucoma			Control vs mild-moderate glaucoma			Control vs severe glaucoma			Mild-moderate glaucoma vs severe glaucoma		
	AUC	Sensitivity	Specificity	AUC	Sensitivity	Specificity	AUC	Sensitivity	Specificity	AUC	Sensitivity	Specificity
Vel constriction inferior quadrant-field	0.620 (0.525, 0.715)	0.304 (0.210, 0.398)	0.913 (0.832, 0.994)	0.620 (0.518, 0.721)	0.264 (0.162, 0.366)	0.935 (0.863, 1.000)	0.621 (0.458, 0.783)	0.400 (0.185, 0.615)	0.913 (0.832, 0.994)	0.502 (0.353, 0.651)	0.400 (0.185, 0.615)	0.722 (0.619, 0.826)
Vel dilation inferior quadrant-field	0.521 (0.422, 0.619)	0.326 (0.230, 0.422)	0.826 (0.717, 0.936)	0.503 (0.397, 0.608)	0.125 (0.049, 0.201)	1.000 (1.000, 1.000)	0.585 (0.423, 0.746)	0.450 (0.232, 0.668)	0.826 (0.717, 0.936)	0.550 (0.401, 0.699)	0.750 (0.560, 0.940)	0.458 (0.343, 0.573)

Data are represented as average (95% CI)
AUC area under the ROC curve, PIPR post-illumination pupil response, T time, Vel velocity

with the perifoveal thickness ($r = -0.290$, $P < 0.001$) and the perifoveal volume ($r = -0.213$, $P = 0.011$) (Fig. 4a).

In response to the superior quadrant stimulus, the time to pupil dilation was negatively correlated to the inferior hemisphere GCC thickness ($r = -0.531$, $P < 0.001$), the inferior parafoveal thickness ($r = -0.232$, $P = 0.006$), the inferior parafoveal volume ($r = -0.284$, $P < 0.001$), the inferior perifoveal thickness ($r = -0.451$, $P < 0.001$), and the inferior perifoveal volume ($r = -0.417$, $P < 0.001$). The PIPR to the superior quadrant stimulus was negatively correlated to the inferior parafoveal thickness ($r = -0.210$, $P = 0.014$), the inferior parafoveal volume ($r = -0.185$, $P = 0.030$), and the inferior perifoveal thickness ($r = -0.205$, $P = 0.016$). The constriction amplitude was inversely correlated to the inferior hemisphere GCC thickness ($r = -0.218$, $P = 0.010$), the inferior perifoveal thickness ($r = -0.207$, $P = 0.014$), and the inferior perifoveal volume ($r = -0.208$, $P = 0.014$).

In response to the inferior quadrant stimulus, the time to pupil dilation was negatively correlated with the superior hemisphere GCC thickness ($r = -0.383$, $P < 0.001$), the superior parafoveal thickness ($r = -0.218$, $P = 0.010$), the superior parafoveal volume ($r = -0.189$, $P = 0.026$), the superior perifoveal thickness ($r = -0.299$, $P < 0.001$), and the superior perifoveal volume ($r = -0.304$, $P < 0.001$). The PIPR to the inferior quadrant stimulus was negatively correlated to the superior parafoveal thickness ($r = -0.273$, $P = 0.001$), the superior parafoveal volume ($r = -0.251$, $P = 0.003$), the superior perifoveal thickness ($r = -0.310$, $P < 0.001$), and the superior perifoveal volume ($r = -0.290$, $P < 0.001$). The dilation velocity in response to the inferior quadrant stimulus was correlated with the superior perifoveal thickness ($r = -0.211$, $P = 0.013$) and volume ($r = 0.203$, $P = 0.207$).

Table 3 summarizes the correlations between pupillometric features and vision field median deviation. In response to the full-field stimulus, the constriction amplitude ($r = -0.372$, $P < 0.001$), constriction velocity ($r = -0.293$, $P < 0.001$), and the dilation velocity ($r = -0.225$, $P = 0.008$) were inversely

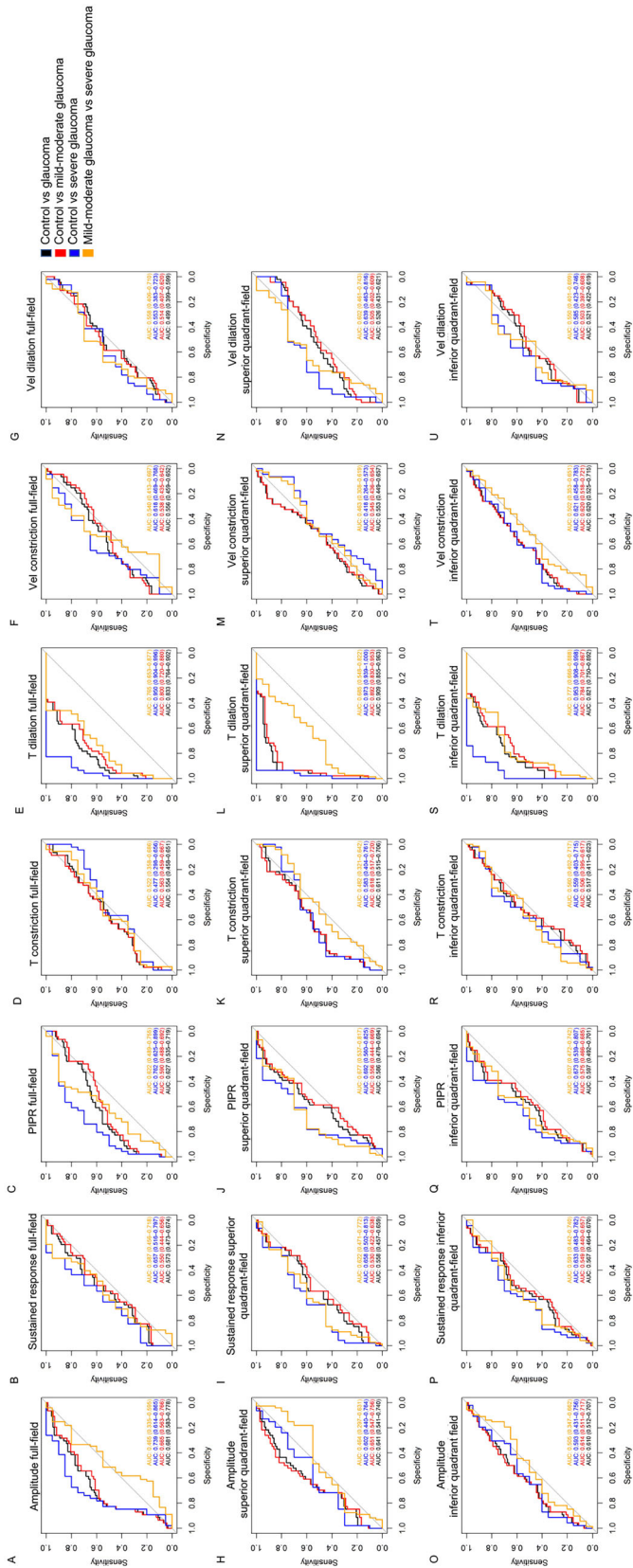


Fig. 5 Diagnostic values of pupillometric features. **a–g** ROC curves of PLR features in full-field stimuli; **h–n** ROC curves of PLR features in superior quadrant-field stimuli; **o–u** ROC curves of PLR features in inferior quadrant-field stimuli. Black line = AUC in discriminating control vs glaucoma, red line = AUC in discriminating control vs mild-moderate glaucoma; blue line = AUC in discriminating control vs severe glaucoma; orange line = AUC in discriminating mild-moderate glaucoma vs severe glaucoma. Data are represented as average (95% CI). ROC receiver operating characteristic curve, AUC area under the ROC curve, T time, Vel velocity, PIPR post-illumination pupil response

correlated to MD score. The post-illumination response ($r = 0.280$, $P < 0.001$) and dilation time ($r = 0.479$, $P < 0.001$) were positively correlated with MD score. In response to the superior quadrant-field stimulus, the post-illumination response ($r = 0.184$, $P = 0.030$) and the dilation time ($r = -0.502$, $P < 0.001$) were positively correlated with the MD score. The dilation velocity ($r = -0.205$, $P = 0.016$) was negatively correlated with MD score. In response to the inferior quadrant-field stimulus, the dilation time ($r = 0.515$, $P < 0.001$) was positively correlated with the MD score, and the velocity in constriction ($r = -0.177$, $P = 0.037$) and velocity in dilation ($r = -0.238$, $P = 0.005$) were negatively correlated with MD score. Overall, the strongest correlations with MD score were the dilation time in response to the inferior quadrant stimulus, followed by the dilation time in response to the superior quadrant and full-field stimulus. The maximum constriction amplitude and PIPR in full-field stimulus also showed moderate correlations.

Diagnostic Performance of Pupillometric Features

Twenty-one pupillometric features were evaluated for the diagnostic performance of glaucoma (Table 4). The ROC curves are presented in Fig. 5. The variable with the greatest AUC was the dilation time in response to the superior quadrant-field stimulus (AUC 0.909, sensitivity 0.837, specificity 0.935), followed by the dilation time in response to the full-field stimulus (AUC 0.833, sensitivity 0.739, specificity 0.761), and the dilation time in response to the inferior quadrant-field stimulus (AUC 0.821, sensitivity 0.696, specificity 0.804). The constriction amplitude (AUC_{full-field} 0.681, sensitivity_{full-field} 0.598, specificity_{full-field} 0.761; AUC_{superior quadrant} 0.641, sensitivity_{superior quadrant} 0.815, specificity_{superior quadrant} 0.435; AUC_{inferior quadrant} 0.610, sensitivity_{superior quadrant} 0.348, specificity_{superior quadrant} 0.870) and PIPR (AUC_{full-field} 0.627, sensitivity_{full-field} 0.554, specificity_{full-field} 0.739; AUC_{superior quadrant} 0.586, sensitivity_{superior quadrant} 0.891, specificity_{superior quadrant} 0.304; AUC_{inferior quadrant} 0.597,

sensitivity_{superior quadrant} 0.859, specificity_{superior quadrant} 0.391) also showed good diagnostic value in three experimental tasks.

DISCUSSION

Using a head-mounted chromatic pupillometer, we conducted measurements of the pupillary response to full-field and sectorial light stimuli and discovered a correlation between PLR features and macular structures in glaucoma. These findings suggest that PLR tests could serve as a rapid and quantitative diagnostic evaluation tool for glaucoma, reflecting the structural macular impairment.

It has long been believed that glaucomatous arcuate damage spares the macular region until the end stage [30]. However, macular measures are of special interest now because of the density of RGCs located in this region and the realization that, contrary to conventional opinion, the macula often is involved early in the glaucomatous process [6, 31, 32]. Structural biomarkers can now be measured in patients with glaucoma in the macula with an increasing number of OCT parameters available [33, 34]. The macular measurements have been shown to possibly be of value for monitoring eyes with advanced glaucoma, beyond the floor observed in circumpapillary retinal nerve fiber layer (cpRNFL) measurements [35]. Wan et al. found that the inner macular thickness could discriminate glaucomatous eyes from healthy eyes even in the early stage [7]. The current study also expands on previous research by analyzing measurements of the inner macula. The inner retinal thickness and volume at the fovea do not alter significantly in patients with glaucoma in our study. The most discriminating parameters are the thickness and volume of the inner retina perifoveal inferior hemisphere. These results are in line with a previous study reporting that the average RGC-related layer shows greater glaucomatous thinning in the inferior retina in patients with or suspected of having glaucoma, since most of the inferior macula projects to the inferior quadrant of the disc, a region known to be particularly vulnerable to glaucomatous damage [31].

Functional glaucomatous progression has both personal and societal costs and therefore has a serious impact on quality of life [36, 37]. The VF examinations, however, are subjective, time-consuming, and lack reproducibility in some circumstances [37–39]. The chromatic pupillometry has been proven useful for objectively evaluating the ipRGC dysfunction in patients with glaucoma [11]. Measurement of the PLR features induced by bright blue light stimuli showed impaired pupillary responses in patients with glaucoma and a reduced post-illumination pupillary response after light offset, representing the melanopsin dysfunction [11, 22–24, 26, 27]. Some studies indicated that the magnitude of the PIPR after exposure to a bright blue light stimulus correlated with the magnitude of visual field loss, and retinal nerve fiber layer (RNFL) thinning [22, 40, 41]. Rukmini et al. showed that the PLR was reduced in patients with POAG at high irradiance levels, associating strongly with disease severity with a significant linear correlation between pupil diameter and mean deviation, as well as cup-to-disc ratio [26]. Gracitelli et al. observed that the sustained pupillary response to the blue flash was associated with the average RNFL thickness as well as VF loss [40]. Although some studies indicated that ipRGCs are relatively resistant to glaucomatous damage and did not decrease until the late stage [25, 40, 42], Najjar et al. showed that patients with early-stage POAG exhibit reduced PLR to moderate and high irradiances of chromatic lights, and the PLR alteration correlates with RNFL thinning but not the VF scores [24]. Using quadrant field stimuli, Adhikari et al. detected attenuated PIPR in individuals with early-stage glaucoma, preperimetric glaucoma, and suspected glaucoma [20]. In this study, we utilized HMDs with binocular screens to conduct the examination (Fig. 1), without the need for an eyepatch or a dark room. Our findings demonstrated that a cost-effective and time-efficient test, which can be performed in simple circumstances, has the potential to detect glaucomatous damage.

Findings from previous studies have primarily focused on the classification performance of PLR for the detection of overall functional loss in glaucoma [23, 24, 27, 40, 41]. In our full-field

stimulus experiment, we found that dilation time back to baseline (AUC 0.833, 95% CI 0.764–0.902) demonstrated better diagnostic performance than constriction amplitude (AUC 0.681, 95% CI 0.583–0.778) and PIPR (AUC 0.627, 95% CI 0.535–0.719). The dilation time in the full-field experiment also showed good performance in discriminating mild–moderate glaucoma from healthy eyes (AUC 0.800, 95% CI 0.720–0.880), and in discriminating mild–moderate glaucoma from severe glaucoma (AUC 0.765, 95% CI 0.653–0.877) (Fig. 5, Table 4). In our study, the glaucoma eyes exhibit sluggish dilation due to afferent defects, a response which could be used to detect or monitor the progression of glaucoma. The altered PLR features in the full-field stimulus are correlated with MD scores (amplitude full-field $r = -0.372$, $P < 0.001$; PIPR full-field $r = 0.280$, $P < 0.001$; T dilation full-field $r = 0.479$, $P < 0.001$). These PLR features also presented a stronger association with parafoveal and perfoveal measurements (Fig. 4a). The patients with glaucoma included in our study are at a relatively early disease stage (MD = 5.65 dB), which suggests that the altered PLR features (amplitude full-field, PIPR full-field, T dilation full-field) in full-field experiments may indicate ipRGC dysfunction or loss, reflecting macular structural damage at an early stage.

Several previous studies used the Ganzfeld dome [24, 26, 40] or the Maxwellian system [20, 43] as the light source in PLR tests, generating a relatively narrow area of the light stimulus. In our study, we used the head-mounted display (110° in diameter), providing stimuli of a larger area. Further, we used the sectorial stimuli to evaluate if the regional structural defect could be detected by chromatic pupillometry. Similar to the finding in the full-field stimulus experiment, the most distinct PLR feature was the time to pupil dilation in response to both quadrant stimuli ($P < 0.001$ in both comparisons), the PIPR to quadrant-field stimulus was decreased in the severe glaucoma group relative to the healthy control group (superior quadrant, $P = 0.018$; inferior quadrant, $P = 0.035$). The alteration in PLRs correlated well with regional macular measurements (Fig. 4B, C), especially the dilation time to

superior and inferior quadrant-field stimulus. These results suggest that the structure–function association between inner macular measurements (parafoveal thickness and volume, perifoveal thickness and volume) and PLR features translates to ipRGC loss or dysfunction at the corresponding region. Of note, we found that the dilation time to superior quadrant stimulus (AUC 0.909, 95% CI 0.855–0.963) and inferior quadrant stimulus (AUC 0.821, 95% CI 0.750–0.892) demonstrated excellent diagnostic accuracy in discriminating glaucoma eyes from healthy eyes. The PLR testing paradigm of our chromatic binocular pupillometry could be used in community settings, general practitioner’s clinics, and in telemedicine, reducing the cost of accurate glaucoma detection. Longitudinal studies could be carried out to further evaluate the potential of chromatic binocular pupillometry in tracking glaucoma progression.

We acknowledge some limitations with our study. First, the PLR to stimuli could not be entirely isolated to the ipRGC circuit. However, the PLR to the melanopsin-weighted stimuli is considered to be weighted by ipRGCs because they participate to a major extent in the response [44]. Second, abnormal PLRs may occur in multiple ocular diseases [8, 10, 11, 44–47] and other systemic diseases [48–51]. For example, previous studies showed that patients with outer retinal disease (retinitis pigmentosa or Leber congenital amaurosis) presented attenuated PLRs to the rod-weighted dim blue light stimulus, as well as weak responses to the cone-weighted red light stimulus. In contrast, the PIPR for the melanopsin-weighted stimulus appeared normal in patients with retinitis pigmentosa or Leber congenital amaurosis [10, 45]. Patients with non-proliferative diabetic retinopathy (NPDR) presented normal PLRs to the rod-weighted stimulus and reduced PLRs to the cone-weighted stimulus. Patients with mild or moderate-to-severe NPDR also presented an attenuated PIPR in the melanopsin-weighted stimulus [47]. In patients with early age-related macular degeneration, PIPR amplitude to melanopsin-weighted stimulus was attenuated, but not the latency or transient amplitude [46]. By comparing different PLR features responding to different stimuli one could distinguish

glaucoma from other diseases. Although this alteration may lower the specificity of pupillometry for glaucoma detection, the ability to detect other diseases is beneficial for screening strategies in opportunistic examinations.

CONCLUSION

The PLRs of glaucomatous eyes are impaired in response to full-field and sectoral light stimulation. The pupil redilation after constriction, the constriction amplitude, and the PIPR are sensitive parameters for the detection of glaucomatous damage. The altered PLR features correlates well with the macular structural change in patients with glaucoma. A major advantage of our approach is that it can be adapted for population screening in compact devices, providing objective data on the integrity of the PLR circuits. A long-term study with both PLR tests and macular structural measurements is required to ascertain the temporal sequence of change in macular structure and PLR features during the development and progression of glaucoma.

ACKNOWLEDGEMENTS

The authors thank all the participants for their valuable contribution to this research.

Funding. The journal’s Rapid Service Fee was supported by the State Key Project of the National Natural Science Foundation of China (No. 82030027 and No. 61831015).

Authorship. All authors meet the International Committee of Medical Journal Editors (ICMJE) authorship criteria, take responsibility for the integrity of the work as a whole, and have given approval for this version to be published.

Author Contributions. Xinghuai Sun and Yadan Quan: conceptualization. Yadan Quan, Huiyu Duan, Zongyi Zhan, Yuening Shen, and Jing Huang: methodology. Yadan Quan, Zongyi Zhan, and Rui Lin: data analysis. Yadan Quan

and Xinghuai Sun: writing—original draft preparation. Tingting Liu, Ting Zhang, Jihong Wu, Huang Jing, Guangtao Zhai, Xuefei Song and Yixiong Zhou: writing, review and editing. Xinghuai Sun and Guangtao Zhai: funding acquisition. All authors contributed to the article and approved the submitted version.

Disclosures. All named authors declare that they have no competing interests.

Compliance with Ethics Guidelines. The study was approved by the human subjects review committee of the Eye and ENT Hospital of Fudan University (No.202267) and all procedures adhered to the tenets of the Declaration of Helsinki. All subjects provided written informed consent before experiment.

Data Availability. The data that support the findings of this study are available from the corresponding author upon reasonable request.

Open Access. This article is licensed under a Creative Commons Attribution-NonCommercial 4.0 International License, which permits any non-commercial use, sharing, adaptation, distribution and reproduction in any medium or format, as long as you give appropriate credit to the original author(s) and the source, provide a link to the Creative Commons licence, and indicate if changes were made. The images or other third party material in this article are included in the article's Creative Commons licence, unless indicated otherwise in a credit line to the material. If material is not included in the article's Creative Commons licence and your intended use is not permitted by statutory regulation or exceeds the permitted use, you will need to obtain permission directly from the copyright holder. To view a copy of this licence, visit <http://creativecommons.org/licenses/by-nc/4.0/>.

REFERENCES

1. Flaxman SR, Bourne RRA, Resnikoff S, et al. Global causes of blindness and distance vision impairment 1990–2020: a systematic review and meta-analysis. *Lancet Glob Health*. 2017;5(12):e1221–34.
2. Jonas JB, Aung T, Bourne RR, Bron AM, Ritch R, Panda-Jonas S. Glaucoma. *Lancet*. 2017;390(10108):2183–93.
3. Kanamori A, Nakamura M, Escano MF, Seya R, Maeda H, Negi A. Evaluation of the glaucomatous damage on retinal nerve fiber layer thickness measured by optical coherence tomography. *Am J Ophthalmol*. 2003;135(4):513–20.
4. Leung CK, Liu S, Weinreb RN, et al. Evaluation of retinal nerve fiber layer progression in glaucoma a prospective analysis with neuroretinal rim and visual field progression. *Ophthalmology*. 2011;118(8):1551–7.
5. Wassle H, Grunert U, Rohrenbeck J, Boycott BB. Cortical magnification factor and the ganglion cell density of the primate retina. *Nature*. 1989;341(6243):643–6.
6. Mohammadzadeh V, Fatehi N, Yarmohammadi A, et al. Macular imaging with optical coherence tomography in glaucoma. *Surv Ophthalmol*. 2020;65(6):597–638.
7. Wan KH, Lam AKN, Leung CK. Optical coherence tomography angiography compared with optical coherence tomography macular measurements for detection of glaucoma. *JAMA Ophthalmol*. 2018;136(8):866–74.
8. Kardon R, Anderson SC, Damarjian TG, Grace EM, Stone E, Kawasaki A. Chromatic pupillometry in patients with retinitis pigmentosa. *Ophthalmology*. 2011;118(2):376–81.
9. Park JC, Moss HE, McAnany JJ. The pupillary light reflex in idiopathic intracranial hypertension. *Invest Ophthalmol Vis Sci*. 2016;57(1):23–9.
10. Park JC, Moura AL, Raza AS, Rhee DW, Kardon RH, Hood DC. Toward a clinical protocol for assessing rod, cone, and melanopsin contributions to the human pupil response. *Invest Ophthalmol Vis Sci*. 2011;52(9):6624–35.
11. Rukmini AV, Milea D, Gooley JJ. Chromatic pupillometry methods for assessing photoreceptor health in retinal and optic nerve diseases. *Front Neurol*. 2019;10:76.
12. Chang DS, Xu L, Boland MV, Friedman DS. Accuracy of pupil assessment for the detection of glaucoma: a systematic review and meta-analysis. *Ophthalmology*. 2013;120(11):2217–25.
13. Lucas RJ. Mammalian inner retinal photoreception. *Curr Biol*. 2013;23(3):R125–33.

14. Yeh CY, Koehl KL, Harman CD, et al. Assessment of rod, cone, and intrinsically photosensitive retinal ganglion cell contributions to the canine chromatic pupillary response. *Invest Ophthalmol Vis Sci.* 2017;58(1):65–78.
15. Aranda ML, Schmidt TM. Diversity of intrinsically photosensitive retinal ganglion cells: circuits and functions. *Cell Mol Life Sci.* 2021;78(3):889–907.
16. Berson DM, Dunn FA, Takao M. Phototransduction by retinal ganglion cells that set the circadian clock. *Science.* 2002;295(5557):1070–3.
17. Dacey DM, Liao HW, Peterson BB, et al. Melanopsin-expressing ganglion cells in primate retina signal colour and irradiance and project to the LGN. *Nature.* 2005;433(7027):749–54.
18. Hattar S, Liao HW, Takao M, Berson DM, Yau KW. Melanopsin-containing retinal ganglion cells: architecture, projections, and intrinsic photosensitivity. *Science.* 2002;295(5557):1065–70.
19. Zhan ZY, Huang YR, Zhao LW, et al. Use of a tissue clearing technique combined with retrograde transsynaptic viral tracing to evaluate changes in mouse retinorecipient brain regions following optic nerve crush. *Neural Regen Res.* 2023;18(4):913–21.
20. Adhikari P, Zele AJ, Thomas R, Feigl B. Quadrant field pupillometry detects melanopsin dysfunction in glaucoma suspects and early glaucoma. *Sci Rep.* 2016;6:33373.
21. Ahmadi H, Lund-Andersen H, Kolko M, Bach-Holm D, Alberti M, Ba-Ali S. Melanopsin-mediated pupillary light reflex and sleep quality in patients with normal tension glaucoma. *Acta Ophthalmol.* 2020;98(1):65–73.
22. Gracitelli CP, Duque-Chica GL, Roizenblatt M, et al. Intrinsically photosensitive retinal ganglion cell activity is associated with decreased sleep quality in patients with glaucoma. *Ophthalmology.* 2015;122(6):1139–48.
23. Najjar RP, Rukmini AV, Finkelstein MT, et al. Handheld chromatic pupillometry can accurately and rapidly reveal functional loss in glaucoma. *Br J Ophthalmol.* 2021;107:663.
24. Najjar RP, Sharma S, Atalay E, et al. Pupillary responses to full-field chromatic stimuli are reduced in patients with early-stage primary open-angle glaucoma. *Ophthalmology.* 2018;125(9):1362–71.
25. Obara EA, Hannibal J, Heegaard S, Fahrenkrug J. Loss of melanopsin-expressing retinal ganglion cells in severely staged glaucoma patients. *Invest Ophthalmol Vis Sci.* 2016;57(11):4661–7.
26. Rukmini AV, Milea D, Baskaran M, et al. Pupillary responses to high-irradiance blue light correlate with glaucoma severity. *Ophthalmology.* 2015;122(9):1777–85.
27. Kelbsch C, Maeda F, Strasser T, et al. Pupillary responses driven by ipRGCs and classical photoreceptors are impaired in glaucoma. *Graefes Arch Clin Exp Ophthalmol.* 2016;254(7):1361–70.
28. Wen W, Zhang P, Liu T, et al. A novel motion-on-color paradigm for isolating magnocellular pathway function in preperimetric glaucoma. *Invest Ophthalmol Vis Sci.* 2015;56(8):4439–46.
29. Andreoli MT, Lim JI. Optical coherence tomography retinal thickness and volume measurements in X-linked retinoschisis. *Am J Ophthalmol.* 2014;158(3):567-73e2.
30. Ramulu P. Glaucoma and disability: which tasks are affected, and at what stage of disease? *Curr Opin Ophthalmol.* 2009;20(2):92–8.
31. Hood DC, Raza AS, de Moraes CG, Liebmann JM, Ritch R. Glaucomatous damage of the macula. *Prog Retin Eye Res.* 2013;32:1–21.
32. Tatham AJ, Medeiros FA. Detecting structural progression in glaucoma with optical coherence tomography. *Ophthalmology.* 2017;124(12S):S57–65.
33. Raza AS, Hood DC. Evaluation of the structure-function relationship in glaucoma using a novel method for estimating the number of retinal ganglion cells in the human retina. *Invest Ophthalmol Vis Sci.* 2015;56(9):5548–56.
34. Nouri-Mahdavi K, Weiss RE. Detection of glaucoma deterioration in the macular region with optical coherence tomography: challenges and solutions. *Am J Ophthalmol.* 2021;222:277–84.
35. Bowd C, Zangwill LM, Weinreb RN, Medeiros FA, Belghith A. Estimating optical coherence tomography structural measurement floors to improve detection of progression in advanced glaucoma. *Am J Ophthalmol.* 2017;175:37–44.
36. Burr JM, Mowatt G, Hernandez R, et al. The clinical effectiveness and cost-effectiveness of screening for open angle glaucoma: a systematic review and economic evaluation. *Health Technol Assess.* 2007;11(41):iii-iv, ix-x, 1–190.
37. De Moraes CG, Liebmann JM, Levin LA. Detection and measurement of clinically meaningful visual field progression in clinical trials for glaucoma. *Prog Retin Eye Res.* 2017;56:107–47.

38. Chien L, Liu R, Girkin C, Kwon M. Higher contrast requirement for letter recognition and macular RGC+ layer thinning in glaucoma patients and older adults. *Invest Ophthalmol Vis Sci.* 2017;58(14):6221–31.
39. Wen Y, Chen Z, Chen S, et al. Higher contrast thresholds for vanishing optotype recognition in macular visual fields among glaucoma patients: a structure-function analysis. *Br J Ophthalmol.* 2022;106(11):1530–7.
40. Gracitelli CP, Duque-Chica GL, Moura AL, et al. A positive association between intrinsically photosensitive retinal ganglion cells and retinal nerve fiber layer thinning in glaucoma. *Invest Ophthalmol Vis Sci.* 2014;55(12):7997–8005.
41. Yoshikawa T, Obayashi K, Miyata K, Saeki K, Ogata N. Association between postillumination pupil response and glaucoma severity: a cross-sectional analysis of the light study. *Invest Ophthalmol Vis Sci.* 2022;63(3):24.
42. Honda S, Namekata K, Kimura A, et al. Survival of alpha and intrinsically photosensitive retinal ganglion cells in NMDA-induced neurotoxicity and a mouse model of normal tension glaucoma. *Invest Ophthalmol Vis Sci.* 2019;60(12):3696–707.
43. Feigl B, Mattes D, Thomas R, Zele AJ. Intrinsically photosensitive (melanopsin) retinal ganglion cell function in glaucoma. *Invest Ophthalmol Vis Sci.* 2011;52(7):4362–7.
44. Kardon R, Anderson SC, Damarjian TG, Grace EM, Stone E, Kawasaki A. Chromatic pupil responses: preferential activation of the melanopsin-mediated versus outer photoreceptor-mediated pupil light reflex. *Ophthalmology.* 2009;116(8):1564–73.
45. Collison FT, Park JC, Fishman GA, McAnany JJ, Stone EM. Full-field pupillary light responses, luminance thresholds, and light discomfort thresholds in CEP290 Leber congenital amaurosis patients. *Invest Ophthalmol Vis Sci.* 2015;56(12):7130–6.
46. Maynard ML, Zele AJ, Feigl B. Melanopsin-mediated post-illumination pupil response in early age-related macular degeneration. *Invest Ophthalmol Vis Sci.* 2015;56(11):6906–13.
47. Park JC, Chen YF, Blair NP, et al. Pupillary responses in non-proliferative diabetic retinopathy. *Sci Rep.* 2017;7:44987.
48. La Morgia C, Romagnoli M, Pizza F, et al. Chromatic pupillometry in isolated rapid eye movement sleep behavior disorder. *Mov Disord.* 2022;37(1):205–10.
49. Narita A, Shirai K, Kubota N, et al. Abnormal pupillary light reflex with chromatic pupillometry in Gaucher disease. *Ann Clin Transl Neurol.* 2014;1(2):135–40.
50. Romagnoli M, Stanzani Maserati M, De Matteis M, et al. Chromatic pupillometry findings in Alzheimer's disease. *Front Neurosci.* 2020;14:780.
51. Tan TE, Finkelstein MT, Tan GSW, et al. Retinal neural dysfunction in diabetes revealed with handheld chromatic pupillometry. *Clin Exp Ophthalmol.* 2022;50(7):745–56.